SPIE Aug 26-30, 2007 San Diego

Toward a complete metrological solution for the mirrors for the Constellation-X spectroscopy x-ray telescope

J. P. Lehan,[a,b] S. Owens,[b] T. Hadjimichael,[b,c] M. Hong,[b,c]
K.-W. Chan,[a,b] T.T. Saha,[b] P. Reid,[d] and W. W. Zhang[b]

[a]Center for Research and Exploration in Space Science and Technology, NASA Goddard Space Flight Center, and Department of Physics, University of Maryland, Baltimore County, 1000 Hilltop Circle, Baltimore, Maryland 21250
[b]NASA Goddard Space Flight Center, Greenbelt, Maryland 20771
[c] Ball Aerospace, 1616 McCormick Drive, Upper Marlboro, MD 20774
[d]Harvard-Smithsonian Center for Astrophysics, 60 Garden Street, Cambridge, MA 02138

ABSTRACT

We present an overview update of the metrological approach to be employed for the segmented mirror fabrication for Constellation-X spectroscopy x-ray telescope. We compare results achieved to date with mission requirements. This is discussed in terms of inherent capability versus in-practice capability.

Keywords: Optical Metrology, x-ray optics, Constellation-X

1.0 INTRODUCTION

1.1 Constellation-X & Spectroscopy X-ray Telescope Overview

The Constellation-X mission[1,2] is a spectroscopic x-ray mission to be flown in 2016 as a compliment to the current Chandra x-ray mission. By combining a higher effective area and greater spectral resolving power, this observatory will be a powerful tool for observing black holes, investigating dark matter, and elucidating galactic evolution.

The mission concept consists of a single spacecraft with four 1.3m, ~12.5 arcsec HPD soft x-ray telescopes (SXT) with ~200 nested, azimuthally segmented shells of grazing incidence mirrors. Each SXT has shells ~0.4mm thick and segmented to ~30° or 60° so as to keep the segment arc length to a maximum of ~20cm. The substrate material is glass (Schott D263) coated with iridium. Details of the segment fabrication are described elsewhere.[3] Each telescope is segmented into 6 inner and 12 outer modules (each with many nested primary/secondary reflector pairs) to ease assmbly. Each SXT focusses onto a microcalorimeter array for x-ray nondispersive spectroscopy.

1.2 Metrology requirements for the segmented x-ray mirrors for the SXT

The requirements are based on the mission error budget presented previously.[4,5] The error budget, however, is not cast in terms of the metrology involved so some manipulation and equivalence adjustments are performed to recast the error budget in terms that are readily elucidated from the metrologic methods themselves. Metrology of the mandrels used for forming the thin glass mirrors present their own unique challenges and are not presented here. Table I lists the salient error budget terms for the mirrors along with the metrology accuracy needed to determine those requirements. The old[6] and new metrology method for each term is also shown. This paper concentrates on the current methods and their performance.

1.3 Instrumental versus in-practice performance

For the thin glass mirrors, the measurement accuracy never reaches the instrumental accuracy. This can be seperated into two primary causes inherent to the problem. The first is static self-weight deformation of the mirrors. This is common in all metrology but is made more severe in the case of the thin glass mirrors where the thickness to width aspect ratio exceeds 1/100. These self-weight deformations exceed or are of the order of the metrology requirements themselves. Thus, discussion of the mirror shape independent of its mount becomes superfluous. It proves necessary to solve both the mount

and measurement problem simultaneously. We delay specific mount discussions to the sections on the measurement methods with which they are associated below.

Table I: Summary of Constellation-X mirror metrology method evolution 2004-2007.

Error Term	Budgeted Error	Metrologic Requirement	Current Metrology Method	Old Metrology Method
Average Radius	100 μm	33 μm	Shack Hartmann/ CCMM	CCMM
Cone angle	30 arcsec	10 arcsec	Shack-Hartmann	CCMM
Roundness error	5 μm RMS	2 μm RMS	Shack-Hartmann/ Null Lens	CCMM
ΔΔR	0.5 μm RMS	0.2 μm RMS	Shack-Hartmann/ Null Lens	CCMM
Average Axial Sag	10μm P-V	3 μm P-V	Null Lens	Fizeau Interferometry
Axial Sag Deviation	0.1μm	0.03 μm	Null Lens	Fizeau Interferometry
Axial Slope irregularity	2.4 arcsec RMS	0.8 arcsec RMS	Null Lens	Fizeau Interferometry
Microroughness	0.5 nm,RMS	0.2 nm,RMS	Mireau Interferometry	Mireau Interferometry
Circumfrential slope error	1.6 arc-sec RMS (shell dependent)	0.5 arc-sec RMS (shell dependent)	Null Lens	NA

The second issue is dynamic stability. Again this is complicated by the mounting method. Inherently, however, vibrational displacements resultant from (unsuppressed) environmental factors can be of similar or larger magnitude to the metrology requirements, further complicating the measurements. Thus, the mount must reduce the excursions of the part or the metrology method must be insensitive to the vibrations. We have adopted both vibration suppression and less vibration sensitive metrology in the various scenarios discussed below.

The other aspect of the dynamic stability is one of timescales. It is important that the timescales of the mirror and mount dynamics can be accomodated by the metrology method. For the mirror metrology there are several timescales involved. The mirror vibrations are a tenth of a second or less, air currents (if applicable) are a few seconds to a minute, the stages used for alignment can drift over a few hours (often vibration driven), and the thermal drift of the apparatus is also several hours to half a day. Because of these timescales, we have found that metrology that can be performed in much less than the air current and stage drift times to be the most repeatable. This is true for both the Shack-Hartmann test §2.1 and the null lens measurement §2.3.

It proves to be the dynamic stability problem that must, in general, be solved first. Once the dynamics have been dealt with, the static deformations can be determined unambiguously and the mount modified as needed to reduce the static deformation to a level acceptable for the error budget term to be determined to the accuracy required.

Reference 6 discusses both the dynamics and statics for the mirrors in some detail so we will not repeat that discussion here. We will mention that the results presented here are influenced by these factors. Of note, however, is that the dynamic influences are now being addressed well enough that they are no longer the dominant source of error in the measurements. Table II shows the error budget terms, metrology method used to measure them, and the in-practice metrology uncertainty achieved to date. In Table II, the in-practice uncertainty includes the influence of the dynamic effects.

2. METROLOGY METHODS

2.1 Grazing-incidence Hartmann Test

The Hartmann test is well known in near-normal-incidence optics.[7] As one goes to grazing incidence, the mirror shrinks to essentially a single circular zone of constant radius. Thus, the grazing-incidence Hartmann test samples the entire radial extent of the mirror but only a small sector azimuthally.

Table II: Summary of error budget terms and current metrology uncertainties. Note these in-practice uncertainties include (and are dominated by) the mirror fixturing.

Error Term	Budgeted Error	Metrology Method	In-Practice Uncertainty	Notes
Average Radius	100 μm	Hartmann/ CCMM	??/20 um	??/2
Cone angle	30 arcsec	Hartmann	??	??
Roundness error	5 μm RMS	Hartmann/ Null Lens	??/0.06 μm RMS	??/1
ΔΔR	0.5 μm RMS	Hartmann/ Null Lens	??/0.04 μm RMS	??/2
Average Axial Sag	10μm P-V	Null Lens	0.004 μm P-V	2
Axial Sag Deviation	0.1μm	Null Lens	0.08 μm P-V	2
Axial Slope irregularity	2.4 arcsec RMS	Null Lens	0.05 arcsec	2
Microroughness	0.5 nm,RMS	Mireau Interferometer	0.2 nm RMS	
Circumfrential slope error	1.6 arc-sec RMS (shell dependent)	Null Lens	0.06 arcsec	2

1. In practice estimated
2. In practice measured

In practice, we employ slits rather than holes as is typical in a normal-incidence Hartmann test (Figure 1). This assures that the mirror is fully illuminated radially and any diffraction effects are from the mirror's limited radial extent rather than the mask itself. The slits are 2 mm wide. Thus, the radial blur and azimuthal blur are a combination of the mirror performance and diffraction.

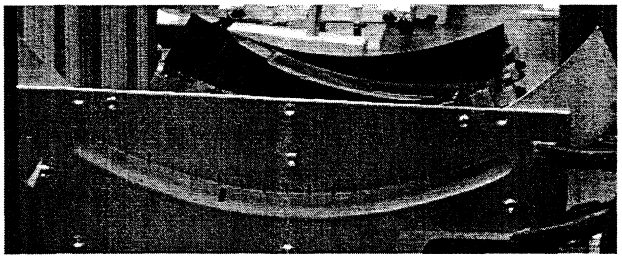

←Figure 1: Grazing-incidence Hartmann mask (foreground) and mirror under test (dark object in middle ground). The mirror is on a self-levelling spring-based low distortion mount.[8]

We currently employ 15 slit positions across a 50 degree azimuthal span. This translates to about a 15 mm center-to-center spacing on the mirror under test for the nominal average radius of 244.5 mm of the prototype mirror segments. A He-Ne laser is spatially filtered and collimated using a high quality off-axis parabola. The mounted mirror segments under test are placed in the collimated beam on a six degree of freedom (6-DOF) stage and the beam folded three times with high quality mirrors until the light comes to focus on a Apogee Instruments, Inc. P47P CCD detector. A narrowband filter is placed in front of the detector to eliminate any stray light from the room.

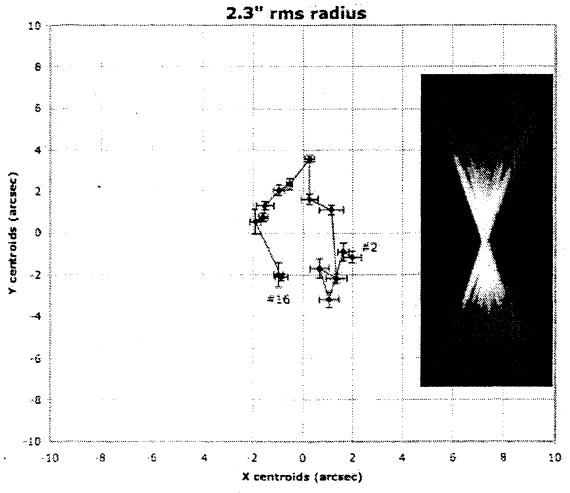

←Figure 2: Example of a grazing-incidence Hartmann diagram for a primary mirror. The full-aperture image is shown in the inset. The rigid- body aberrrations of defocus and coma are apparent, along with smaller residual errors in the part itself.

The detector is initially placed at the nominal focal length (8.5 m for the secondary or 17 m for the primary) and the mirror adjusted using the 6-DOF until a best image is formed. The data are a set of centroids versus azimuthal angle as shown in Fig. 2. This information is fed into a program that determines, via a least-squares fit, the lowest-order positioning errors relative to the collimated beam. From these data the roundness and average cone angle can be extracted. From the residual of the fit, the ΔΔR and circumfrential slope error for the part under test can be determined.

In practice the performance of this test is limited by the mounting of the mirror segment. At the present time, the mirror is

laid horizontally on a self-levelling spring-based mount[8] seen in Figure 1 and this is mounted to the 6-DOF stage. The self-levelling mount relies on the gravity vector being nearly vertical along the centerline of the part so the adjustments made with the 6-DOF stage result in the gravity verctor varying from the original configuration which results in the part moving in the mount in an undesirable way (not the way one wishes it to move given the 6-DOF adjustment). This is prevented by a light tack bond with GE® RTV159 at 4 points at the periphery of the mirror. The bonding process is monitored with the Hartmann aparatus itself to minimize the (local) distortion introduced. This process is estimated to typically modify the Hartmann pattern by XX arcsec RMS.

This technique is still under development as of this writing so that the figures quoted in Table II are estimates based on the data sets available as of this writing.

2.2 Cylindrical coordinate measauring machine (CCMM)

We employ a custom designed non-contact coordinate measuring machine in a cylindrical geometry for determination of the large-scale geometry of the mirrors (Figure 3).[6] This CMM employs a confocal optical probe developed by Stil based on the variation of longitudinal chromatic aberration. A spectum is obtained from the illuminated spot on the sample. This spectrum can be analyzed to obtain a precise distance relative to the calibrated probe. There is a significant tradeoff between measurement range and precision. Our version uses Stihl's highest sensitivity probe, with a quoted ~2nm rms distance uncertainty and ~20 micron total accessable range. It employs high precision stages for radial position, vertical position, and azimuthal position with a radial noise of ~XX nm rms. This is less than the goal for the instrument but still exceeding other non-contact probes. A calibration flat is mounted at a separate azimuthal position adjacent to the test part. This allows calibration (linearization) of the portion of the stage travel of interest for both the radial and vertical stages.

The high data rate of the optical probe (2 kHz) allows dynamic studies of individual points on the mirrors. This compliments the interferometeric measurements (§2.3) and can be employed in the verification of the resonance frequencies of the mirrors in a variety of fixtures.

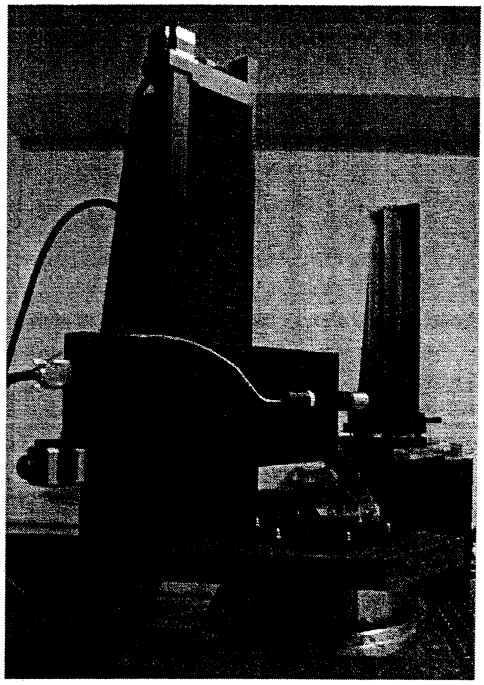

Figure 3: Non-contact Cylindrical Coordinate Measuring Machine (CCMM). The optical probe is attached to precison rotation, radial and z linear stages. The calibration flat is shown on the right but the part under test is not shown in this photograph.→

The performance of the system is limited in practice by three factors: mirror vibration, mirror alignment stage movement, and thermal drift. The latter two factors are a result of the measurement time required for adequate sampling of an entire mirror. Each point requires sufficient samples to average over the vibrations at that point. Thus, the measurement of an entire mirror takes several hours to complete. In principle, the instrument can measure almost all oth the mirror parameters in Table II. To accomplish this to the needed precision, however, the allowable drift of only tens of nm in the stages over that time is required. In addition, the thermal stability needs to be of the same order over a similar timeframe. As of now, we have not been able to achieve the combination of mount and thermal stability to the required level to measure all parameters with the required precision.

There is an additional factor that affects the utility of the CCMM. There is a mathematical degeneracy between cone angle and tilt angle of the segmented mirror relative to its axis. This indeterminancy is a function of the the azimuthal span of the mirror and disappears for a full 360 degree shell.

In spite of these challenges, however, the achievable precision is sufficient to determine the average radius of the parts. The precision for this parameter has been found to be about 20 μm, below the requirement of Table I. The other parameters extracted from the CCMM data serve as a doublecheck for the parameters extracted from the Shack-Hartmann measurements.

2.3 Refractive null lens and strobe Fizeau interferometer

The combination of refective null lens and strobe interferometer covers the figure of the mirrors in the spatial period band from 200 mm to 1 mm. This normal incidence metrological technique enables a much greater spatial fidelity of the mirror surface than practical with the grazing-incidence Shack-Hartmann technique or CCMM. Although the null lens is compatible with any commercial Fizeau interferometer with a sufficiently large collimated beam (>225 mm diameter here), we employ a 4D Technologies FizCam1500® with a 250 mm aperture. This strobe interferometer typically operates at 0.2 msec staring time and a frame rate of 15 frames per second when performing our measurements. This limits the sampling of vibrational frequencies to only 7.5 Hz. Figure 4 illustrates the null lens and strobe Fizeau in use.

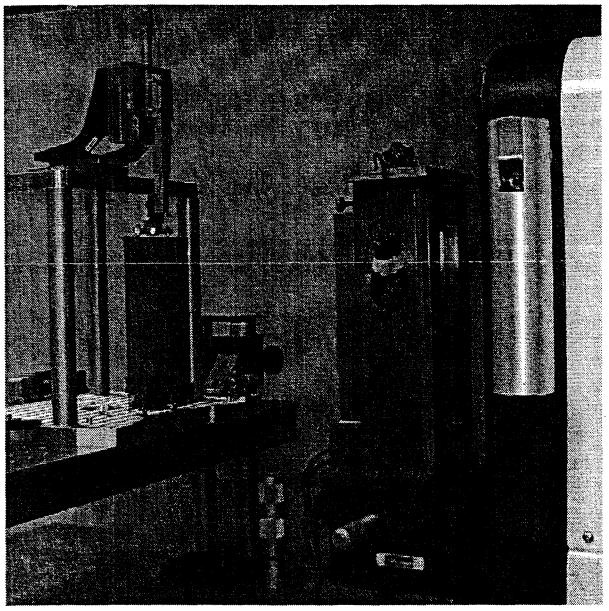

←Figure 4: Cylindrical null lens and strobe Fizeau interferometer measuring mirror. Interferometer is to the far right (in the foreground), the cylindricall null lens is in the right center, and part under test and metrology mount on the left.

The null lens is cylindrical in geometry and its design has been discussed previously.[9] Of note here is that the refractive triplet cyclindrical lens is capable of accommodating the cone angles of any of the telescope's mirrors. This has the advantage over other methods like diffractive optics that only a single lens is needed -- saving time and money but with the distinct disadvantage that the cone angle is not determined. Ways of circumventing this are discussed in an allied paper in these proceedings.[10]

The calibration of the null lens and interferometer flat is performed in the usual way for interferometric systems. Where interferometry on thin glass mirrors deviates from conventional interferometry is that good reproducibility requires extraordinary effort to achieve. The causes of non-reproducability in our case can be divided into two categories: dynamic and static.

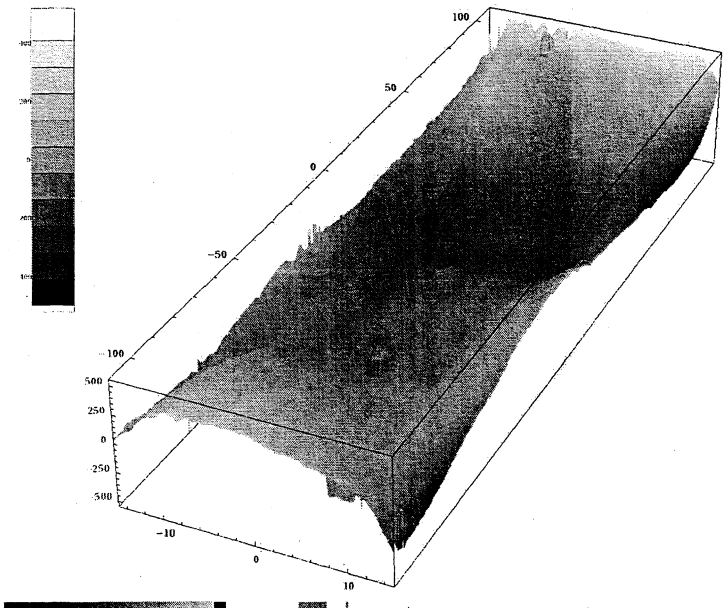

←Figure 5(a): Typical surface map obtained from the average of 100 such maps taken with the set-up shown in Fig. 4. Axial scale ranges from -100 to 100 mm and the azimuthal scale is -15 to 15 degrees in the figure to the left.

The dynamic variations are due to vibration as discussed in §1.3 and air currents. We reduce air currents with curtains to create a static air environment and eliminating heat souces within the curtains (only the laser in the interferometer remains a source of any significance). This appraoch seems to be adequate.

For vibration we take two complimentary tacks. The first is the conventional metrologic approach of isolating environmental vibrations (vibration isolation tables and the like). We have found, however, that this approach is insufficient with reasonble effort for the vibrations. have found, however, that this approach is insufficient with reasonble effort for the vibrations. Our thin mirror's vibrational amplitudes are large even for small vibrational impulses. The second approach is to measure the mirror while vibrating and average out the vibrations. We employ the law of large numbers to tackle this because the environmental sources of vibration are random in time, amplitude and frequency content. Figure 5(a)

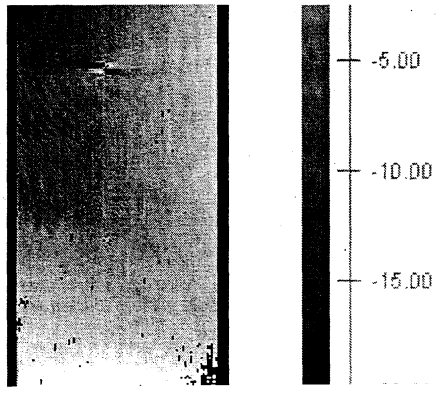

←Figure 5(b): Difference plot between two subsequent averages for 100% of the null

lens clear aperture. RMS error is 5.9 nm. Note the dominant residual seen is probably due to air currents

shows a typical average result whereas 5(b) shows the difference between two such averages with 5 nm rms differnce indicating good averaging by this method.

The static portion of the non-reproducability dominates the overall non-reproducability after the avering process is implemented and it is governed by fixturing. We employ a kinematic mount with the part in a vertical orientation (see Figure 4). The vertical orientation was chosen because it is the minimum deflection orientation since the self-weight deflection is due to column buckling. Because the part is actually a sagged cone rather than a cylindrical shell, however, only the centerline of the mirror is truly vertical during measurement so the periphery of the mirror sees a slightly greater fraction of the gravitation force normal to its surface than the centerline. There is a unique tilt angle that minimizes this P-V variation across the part that is slightly off vertical but the centerline vertical geometry is used in practice because it is easier to find precisely and repeatably.

The mount consists of bearings and fulcrums and is somewhat akin to a two-dimensional Wiffle tree. The bearings accommodate the possibility of locally varying slopes along the perimeter of the mirror without distorting the mirror. In the limit, it reduces to a three-point kinematic mount similar to that discussed in Reference 6. The mount is discussed in more detail in an allied publication.[10]

The net variation caused by repeated mountings and dismountings is much greater than that from the residual uncertainty resultant from vibration when averaging is performed. The combined variability from all causes has been measured to be about 25 nm RMS. This translates to 0.08 μm P-V (worst case) for the axial sag deviation (see Table II). This is below the requirement but still a bit above the metrologic goal (see Table I). Further optimization of the mount should allow us to achieve the metrologic goals on all the quantities measured with the null-lens-strobe-interferometer combination in the near future.

2.4 Mireau interferometry

We employ a Mireau interferometer to measure the mirrors at spatial periods 1 mm to 1 μm. We employ two models (a Zygo NewView® and an ADE Phase Shift MicroXam®). The mirrors are sampled on a 5 x 5 grid and assumed statistically stationary in this spatial period regime. The gravity distortions appear only as tilt in this spatial period band so fixturing is greatly simplified. Performance of both instruments is comparable and we are regularly achieving the performance expected from the manufacturers' specications.

3. Summary and Conclusions

We presented the error budget and associated metrologic goals for the Constellation-X mirror segments. The metrology requirements and an updated implementation plan to meet the particular requirements for metrology on next generation ultralightweight segmented x-ray optics. The principal new metrology developments include a refractive null lens and strobe interferometer, a vertical kinematic fixturing scheme to hold the optics for optical metrology with improved vibrational characteristics, and a grazing-incidence version of the classic Shack-Hartmann test for low order figure determination. This metrology set is at or near the metrology goals for the mission. Futher refinement of the mirror fixturing should put all the measurements comfortably in the regime of meeting the metrology uncertainty goals in the near future.

ACKNOWLEDGEMENTS

This work is funded through the Constellation-X technology development program. This work represents the contributions of numerous people beyond the author list. In particular we wish to acknowledge Dr. David Content for his many years of leadership in this metrology effort, Ms. Linnette Kolos and Mr. Dale Arbogast for technical support; along with SAO (W. Podgorski and W. Davis among others) for valuable analyses. Mention of trade names or commercial products does not constitute endorsement or recommendation by the authors or NASA.

REFERENCES

[1] For an overview, see the description of Constellation-X online at http://constellation.gsfc.nasa.gov

[2] R. Petre, N. E. White,H. D. Tananbaum, A.E. Horschemeier, J. Bookbinder, M.R. Garcia, and J. Grady, "Status of the Constellation-X Mission," Proc. SPIE 6686 6686-10 (2007). [These proceedings]

[3] W. W. Zhang, et al ,"Constellation-X mirror technology development status and plan,", Proc. SPIE 6688 6688-01 (2007). [These proceedings]

[4] William A. Podgorski, Jay Bookbinder, David A. Content, William N. Davis, Mark D. Freeman, Jason H. Hair, Scott M. Owens, Robert Petre, Paul Reid, Timo T. Saha, Jeffrey W. Stewart, and William W. Zhang, "Constellation-X spectroscopy x-ray telescope optical assembly pathfinder image error budget and performance prediction," Proc. SPIE 5168, 318 (2004).

[5] P. Reid, R. Cameron, L. Cohen, M. Elvis, P. Gorenstein, D. Jerius, R. Petre, W. Podgorski, D. Schwartz, and W. Zhang, "Constellation-X to Generation-X: Evolution of large collecting area moderate resolution grazing incidence x-ray telescopes to larger area, high resolution, adjustable optics," SPIE Proc. 5488, 325 (2004).

[6] D. A. Content, D. Colella, T. Hadjimichael, J. P. Lehan, J. McMann, P. B. Reid, T. T. Saha, and W. W. Zhang, "Optical metrology for the segmented optics on the Constellation-X spectroscopy x-ray telescope," Proc. SPIE 5488, 272 (2004).

[7] I. Ghozeil in *Optical Shop Testing*, D. Malacara (ed.),Wiley, New York, pp.323-349,(1978).

[8] W. W. Zhang, K.-W. Chan, J. P. Lehan, and R. Petre, "Fabricate and assemble: an alignment and integration method for next generation x-ray telescopes," Proc. SPIE 6266, 62661M (2006).

[9] J. P. Lehan, T. Hadjimichael, D. A. Content, and W. W. Zhang ,"Design and fabrication of refractive nulls for testing the segmented mirrors of the Constellation-X spectroscopy x-ray telescope (SXT)," Proc. SPIE 5900, 59001D (2005).

[10] J. P. Lehan, T. Hadjimichael, and C. Skocik, "Testing of the mirrors for the Constellation-X spectroscopy x-ray telescope with a refractive null," Proc. SPIE 6688 6688-36 (2007). [These Proceedings]

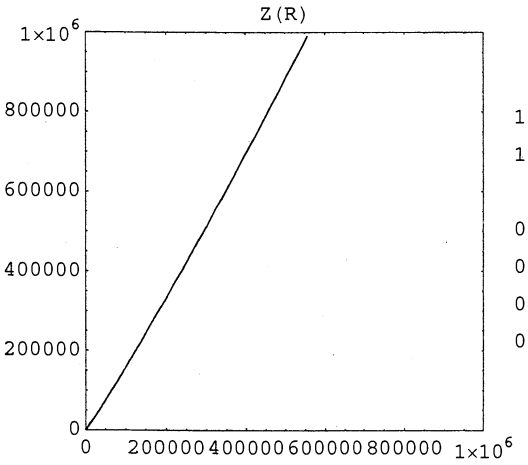
Z(R)
1×10^6
800000
600000
400000
200000
0
0 200000 400000 600000 800000 1×10^6

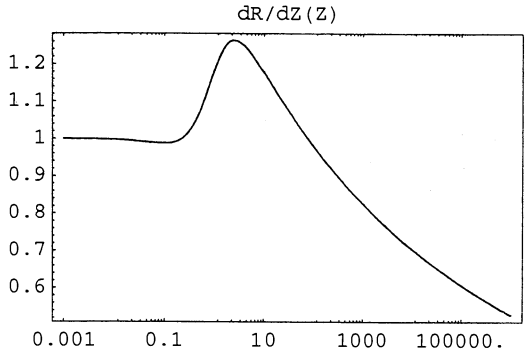
dR/dZ(Z)
1.2
1.1
1
0.9
0.8
0.7
0.6
0.001 0.1 10 1000 100000.

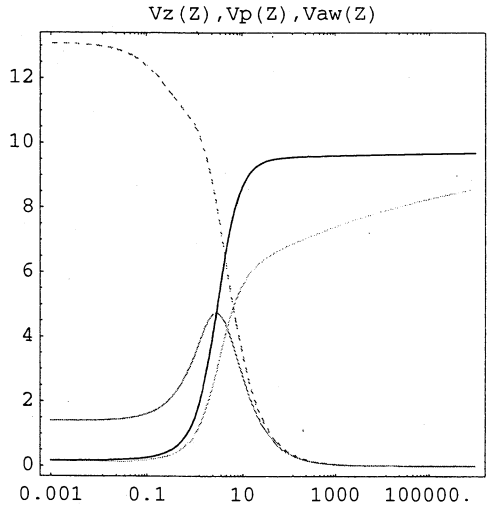
Vz(Z),Vp(Z),Vaw(Z)
12
10
8
6
4
2
0
0.001 0.1 10 1000 100000.

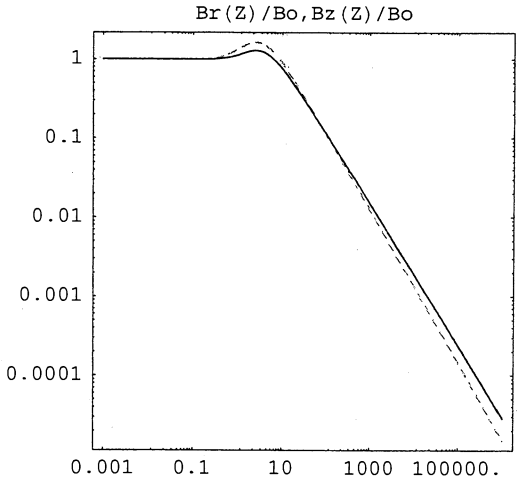
Br(Z)/Bo,Bz(Z)/Bo
1
0.1
0.01
0.001
0.0001
0.001 0.1 10 1000 100000.

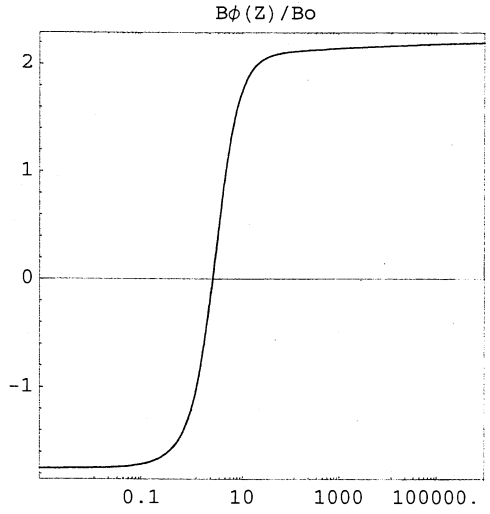
Bϕ(Z)/Bo
2
1
0
-1
0.1 10 1000 100000.